J. COMBIN. MATH. COMBIN. COMPUT. 125 (2025) 2745--2759

Journal of Combinatorial Mathematics and Combinatorial Computing
www.combinatorialpress.com/jcmcc

Research on Innovation Strategy and Practice of Environmental Art Design for Digital Transformation

Qingqing Huo[1,✉]

[1] College of Digital Technology and Design, Shanghai Sipo Polytechnic, Shanghai, 201300, China

ABSTRACT

With the deep development of digital transformation, the field of environmental art design is experiencing unprecedented changes. In this study, under the 3D scene reconstruction algorithm, the feature points of environmental art design images are collected and extracted using the camera self-calibration algorithm, and the shape and topology of the point cloud dataset interpolated surfaces are explored using the triangular meshing algorithm. The rotation matrix is obtained by optimising the internal and external parameters of the camera using the essential matrix, basis matrix and Kruppa's equation to clarify its effect on the efficiency of digital feature extraction of images in the process of environmental art design. The results show that the mesh surfaces constructed by the algorithm proposed in this paper make better use of the point cloud data when the number of cloud points input for environmental art design is the same. The rotation matrix algorithm used in this paper can increase the correct matching point pairs of the data, reduce the false matching point pairs, reduce the false matching rate, reduce the matching time, and eliminate more false matching points. And the triangular grid formed by this method is more uniform, and the quality of the grid is improved. In addition, the average satisfaction ratings of the subjects on the nine secondary test indicators are 4.45, 4.95, 4.75, 4.18, 4.70, 4.60, 4.44, 4.50 and 4.40, respectively. It can be seen that the effect of the application of the digital transformation of the 3D model proposed in this paper has been affirmed.

Keywords: 3D scene reconstruction, camera self-calibration, triangular meshing algorithm, Kruppa equation, environmental art design

1. Introduction

Environmental art design is the use of artistic means, the indoor and outdoor space of the building two parts of the integration of transformation, the use of which can improve the comfort of the residents of the building, the daily life of the feeling has a great impact [1-4]. The concept of environmental art design is relatively broad, it includes the design of indoor environment, outdoor environment, and also includes architectural garden design. The development of information technology has had a profound

✉ Corresponding author.
E-mail address: huo821096@163.com (Q. Huo).
Received 20 February 2024; Revised 05 April 2024; Accepted 20 November 2024; Published Online 15 April 2025.
DOI: 10.61091/jcmcc127a-155

impact on the way of human production, lifestyle, way of thinking and so on [5-8], in this context, the digital transformation of environmental art design is inevitably the future direction of environmental upgrading and development, and if the two can be organically integrated, it can effectively improve the level of environmental art design and promote the overall progress of China's design industry [9-10].

Digital environmental art design is through digital technology and creative expression, design and display of art works of a design approach. It combines art and technology, through digital media and interactivity, presenting a new form of art and experience [11-13]. Digital environmental art design is not only an extension of traditional design, but also an innovative way of expression, with high artistic value and cultural connotation. The significance of digital environmental art design is to bring a new art experience and interactive participation for the audience, breaking through the restrictions of traditional art forms, so that the audience can interact with the art works in real time and participate in the creative process [14-17]. At the same time, digital environmental art design also provides designers with a broader creative space and possibilities, so that they can express more creativity and ideas through technological means [18-20].

In this study, the intrinsic matrix, the basis matrix and the Kruppa equation are used to determine the internal and external parameters of the camera self-calibration algorithm. The acquisition of scattered points in the environmental art and design images is carried out by rotating the matrix. After that 3D reconstruction algorithm is used to get the interpolated surface of irregular shapes of environmental design of cloud data. On the triangular meshing algorithm, the digital transformation of the point cloud data on the surface of the image in the process of environmental art design is carried out by tangent plane fitting, projection and rotation. Finally, the performance of the 3D reconstruction algorithm on environmental art design images and the effect of digital transformation are verified.

2. 3D scene reconstruction algorithm for environmental art design in digital transformation

Extracting three-dimensional information from two-dimensional images, reconstructing the three-dimensional model of environmental art design, and restoring the visual appearance for the reconstructed three-dimensional model are the basic ideas based on the three-dimensional reconstruction method of environmental art design images. According to the degree of regularity of the shape of the environment, the shape of the environment to be modelled can be divided into regular and irregular shapes. Regular objects have relatively simple shapes and convex structures without occlusion. Irregular objects, on the other hand, usually consist of multiple surfaces with irregular shapes and non-smooth surfaces.

Irregular bodies have more complex shapes and have no obvious features. Scattered point clouds are formed after reconstruction, so its modelling process is more complicated than that of regular shapes. In this paper, the contour information of environment design images is extracted by processing a series of images acquired from non-regular target environments. The 3D mesh surface model of the environment is reconstructed by searching the surface points of the environment design image.

2.1. Camera self-calibration algorithm based on environmental image acquisition

The camera self-calibration method [21-22] does not require a calibration reference, and can directly use the constraint relations obtained from the environmentally designed image sequences to compute the parameters of the camera, which is characterised by good real-time performance, and has been a hot issue for research in the field of camera calibration in recent years. In this paper, we adopt the camera self-calibration technique to find the internal and external parameters of the camera using the essential matrix [23], the basis matrix [24-25] and Kruppa's equation.

Since the internal parameter matrix K holds with the basis matrix F with the following relationship:

$$F = K^{-T} E K^{-1} \tag{1}$$

The internal parameter matrix of the camera can be derived from the basis matrix F, which is usually solved by an eight-point algorithm.

The Kruppa equation was first introduced to computer vision by Faugeras and Maybank and applied to the camera self-calibration process. Absolute quadratic curves are closely related to camera calibration and motion estimation. The projection of the absolute quadratic curve on the ambient image plane is also quadratic under strict displacement, and the coordinate equations do not depend on the translation and rotation of the camera, but only on the internal parameters of the camera. The absolute quadratic curve equation on the ambient image plane can be written in matrix representation as:

$$B = K^{-T} K^{-1} \tag{2}$$

Since $A = B^*$ (A is called the Kruppa matrix), with a difference of one constant factor, there is $A = KK^T$. From the Kruppa matrix, the internal parameter matrix of the camera can be derived.

The Kruppa matrix holds with the following derived relational equation:

$$FAF^T = \lambda [e]_x A [e]_x^T \tag{3}$$

where e is the outer pole. We use the simplified Kruppa equation, which avoids the use of epipolar points, which are more difficult to estimate accurately due to noise effects. Firstly the singular value decomposition of the basis matrix F with $F = SDU^T$, is performed:

$$F^T e = UD^T S^T e = 0 \tag{4}$$

where e can be expressed as $e = \mu Sm$, μ is a non-zero constant, $m = (0,0,1)^T$, and so $[e]_x$ can be expressed as:

$$[e]_x = \mu \det(S) S^{-T} [m]_x S^{-1} = \mu S [m]_x S^T \tag{5}$$

where $[m]_x = \begin{pmatrix} 0 & -1 & 0 \\ 1 & 0 & 0 \\ 0 & 0 & 0 \end{pmatrix}$, is obtained by substituting equation (5) into (3):

$$FAF^T = \lambda \mu S [m]_\pi S^T A \mu S [m]_\pi^T S^T = \lambda S [m]_x S^T A S [m]_x^T S^T \tag{6}$$

where $\lambda = \lambda \mu^2$, is obtained by substituting $F = SDU^T$ into the left side of Eq. (6):

$$SDU^T AUD^T S^T = \lambda S [m]_x S^T A S [m]_x^T S^T \tag{7}$$

Multiplying the left and right sides of equation (7) by S^T and S, respectively, gives:

$$DU^T AUD^T = \lambda^T [m]_x S^T A S [m]_x^T \tag{8}$$

Equation (8) is the simplified form of Kruppa's equation.

S is denoted as (s_1, s_2, s_3), where (s_1, s_2, s_3) is the column vector of S, and U is denoted as (u_1, u_2, u_3), where, u_1, u_2, u_3 is the column vector of U, and $D = diag(r, l, 0)$, where r, l are the singular values of FF^{T}, which are obtained by substituting into both sides of (8):

$$DU^T AUD^T = \begin{pmatrix} r & 0 & 0 \\ 0 & l & 0 \\ 0 & 0 & 0 \end{pmatrix} (u_1, u_2, u_3)^T A (u_1, u_2, u_3) \begin{pmatrix} r & 0 & 0 \\ 0 & l & 0 \\ 0 & 0 & 0 \end{pmatrix} \tag{9}$$

Organised:

$$DU^T AUD^T = \begin{pmatrix} r^2 u_1 A u_1 & rl u_1^T A u_2 & 0 \\ lr u_2^T A u_1 & l^2 u_2^T A u_2 & 0 \\ 0 & 0 & 0 \end{pmatrix} \tag{10}$$

$$
\begin{aligned}
&[m]_x S^T AS [m]_i^T = \begin{pmatrix} 0 & -1 & 0 \\ 1 & 0 & 0 \\ 0 & 0 & 0 \end{pmatrix} (s_1, s_2, s_3)^T \\
&A(s_1, s_2, s_3) \begin{pmatrix} 0 & 1 & 0 \\ -1 & 0 & 0 \\ 0 & 0 & 0 \end{pmatrix}
\end{aligned}
\tag{11}
$$

Organised:

$$
[m]_x S^T AS [m]_x^T = \begin{pmatrix} s_2^T As_2 & -s_2^T As_1 & 0 \\ s_1^T As_2 & s_1^T As_1 & 0 \\ 0 & 0 & 0 \end{pmatrix}
\tag{12}
$$

From the above relational equation, we can get the equation about matrix A:

$$
\frac{s_1^T As_1}{l^2 u_2^T Au_2} = \frac{s_2^T As_2}{r^2 u_1^T Au_1} = \frac{s_1^T As_2}{Iru_2^T Au_1} = \frac{-s_2^T As_1}{rlu_1^T Au_2}
\tag{13}
$$

Without considering the camera lens saki change and moving the centre point of the pixel coordinate system to the centre of the environmental art design image, the internal parameter matrix K of the camera can be expressed as $\begin{pmatrix} a_u & 0 & 0 \\ 0 & a_r & 0 \\ 0 & 0 & 1 \end{pmatrix}$, and the Kruppa matrix $A = diag\left(a_v^2, a_v^2, 1\right)$, substituting A into Eq. (13), can be split into a system of two binary quadratic equations as follows:

$$
\begin{cases}
a_{11}X^2 + a_{12}XY + a_{13}Y^2 + a_{14}X + a_{13}Y + a_{16} = 0 \\
a_{21}X^2 + a_{22}XY + a_{33}Y^2 + a_{24}X + a_{23}Y + a_{26} = 0
\end{cases}
\tag{14}
$$

where the internal parameters of the camera are:

$$
\begin{cases}
X = a_4^2 \\
Y = a_v^2 \\
a_{11} = -r^2 u_{11}^2 s_{21} s_{11} - rlu_{11} u_{21} s_{21}^2 \\
a_{12} = -r^2 u_{11}^2 s_{22} s_{12} - r^2 u_{12}^2 s_{21} s_{11} - rlu_{11} u_{21} s_{22}^2 - rlu_{12} u_{22} s_{21}^2 \\
a_{13} = -r^2 u_{12}^2 s_{23} s_{12} - rlu_{12} u_{22} s_{22}^2 \\
a_{14} = -r^2 u_{11}^2 s_{23} s_{13} - r^2 u_{13}^2 s_{21} s_{11} - rlu_{11} u_{21} s_{23}^2 - rlu_{13} u_{23} s_{21}^2 \\
a_{15} = -r^2 u_{12}^2 s_{23} s_{13} - r^2 u_{13}^2 s_{22} s_{12} - rlu_{12} u_{22} s_{23}^2 - rlu_{13} u_{23} s_{22}^2 \\
a_{16} = -r^2 u_{13}^2 s_{23} s_{13} - rlu_{13} u_{23} s_{23}^2 \\
a_{21} = r^2 u_{11}^2 s_{11}^2 - l^2 u_{21}^2 s_{21}^2 \\
a_{22} = r^2 u_{11}^2 s_{12}^2 + r^2 u_{12}^2 s_{11}^2 - l^2 u_{21}^2 s_{22}^2 - l^2 u_{22}^2 s_{21}^2 \\
a_{23} = r^2 u_{12}^2 s_{12}^2 - l^2 u_{22}^2 s_{22}^2 \\
a_{24} = r^2 u_{11}^2 s_{13}^2 + r^2 u_{13}^2 s_{11}^2 - l^2 u_{21}^2 s_{23}^2 - l^2 u_{23}^2 s_{21}^2 \\
a_{25} = r^2 u_{12}^2 s_{13}^2 + r^2 u_{13}^2 s_{12}^2 - l^2 u_{22}^2 s_{23}^2 - l^2 u_{23}^2 s_{22}^2 \\
a_{26} = r^2 u_{13}^2 s_{13}^2 - l^2 u_{23}^2 s_{23}^2
\end{cases}
\tag{15}
$$

Solving the above system of equations, the internal parameters of the camera can be obtained.

Since in this paper, the camera coordinate system is coincided with the world coordinate system in the reconstruction process, and the position of the camera is unchanged in the process of environmental image acquisition, the object is fixed on the rotating platform, and the acquisition of the environmental image is carried out through the rotation of the platform, the translation vector t is 0 and the rotation matrix R is denoted as:

$$R = \begin{pmatrix} 1 & 0 & 0 \\ 0 & 1 & 0 \\ 0 & 0 & 1 \end{pmatrix} \tag{16}$$

2.2. 3D reconstruction algorithm based on feature extraction of environmental surface points

A surface point of an environmental art design image is not actually a point, but rather a small cube that is on the surface of the environmental image. So, the way to determine a surface point can be described as follows: if the small cube is partly in the shadow and partly out of the shadow, then the small cube is defined as a surface point of the environment image. A 6-connection approach is used here. That is, given a point in space, to determine whether the point is a surface point of the environment image, search and determine the points in 6 directions around the point, i.e., assuming that the 3D coordinates of the point in space are (x, y, z), using the 6-connected approach, the values of the 3D coordinates of the points in the 6 directions around it are:

$$\begin{gathered} (x, y, z+d),(x, y, z-d),(x, y+d, z) \\ (x, y-d, z),(x+d, y, z),(x-d, y, z) \end{gathered} \tag{17}$$

where d is the step size. Out of these 6 points, point (x, y, z) is a surface point of the environment image if at least one of the points is an external point of the object and at least one of the points is an internal point of the object.

The projection of a spatial point on the set of image slices by the 3D reconstruction algorithm [26] allows to determine whether the point exists inside the environmental image. Define $M(p,l)$ as the projection function of spatial point p on image slice l with value domain $(1,0)$, i.e., p whether the projected point (x, y) on image slice l is in the shadow or not. Define $I(p)$ as the judgement function of the internal point of the environment image, if $\sum_{l \in L} M(p,l) \geq t$, then $I(p)=1$, then the space point p is the internal point of the environment image; if $\sum_{l \in L} M(p,l) < t$, then $I(p)=0$, then the space point p is the external point of the environment image. $t \leq |L|$, t is the set threshold, L is the set of images l. For a given spatial point, the $I(p)$ function can be used to determine whether it is inside the environment image.

2.3. Triangular meshing of environmental surface point cloud data

Triangular meshing of point cloud data [27] is to form a triangular mesh by interconnecting the data points with triangles, given a set of point cloud data. In essence, the triangular mesh reflects the topological connectivity between the data points and their neighbours. Correct topological connections will effectively reveal the shape and topology of the environmental art design surface embedded in the point cloud data set. The triangular meshing of point cloud data is not only an important basis for constructing the interpolated surface of environmental design with point cloud data, but also plays a great role in promoting the research of new technologies such as visualisation of 3D environmental data field and rapid prototyping. The local area where any point in the point cloud is located can be approximated as a plane, and projecting the point cloud in the 3D local space to the 2D plane for data processing can improve the efficiency of point cloud data processing and reduce the complexity of point cloud processing.

2.3.1. Tangent plane fitting The k-neighbourhood search of point cloud data is a prerequisite for point cloud tangent plane fitting, and it is very inefficient to search the neighbourhood points of a point directly from the point cloud. The kd-tree is a data structure often used in computer science, which is very useful for interval and neighbourhood search. Therefore, in this paper, we establish the kd-tree of a scattered point cloud to achieve the fast finding of k-neighbourhood points of the point cloud.

Let the equation of the tangent plane of the k-neighbourhood point of point p be:

$$ax + by + cz + e = 0 \tag{18}$$

where a, b and c are the components of the normal vector to the tangent plane. Let $a^2 + b^2 + c^2 = 1$, i.e., unitise the plane normal vectors, then the distance from any point $\{p_i(x_i, y_i, z_r), i = 1, 2, \cdots k\}$ in the k-neighbourhood point to the tangent plane is:

$$d_t = |ax_i + by_t + cz_t + e| \tag{19}$$

Based on the principle of least squares when $S = \sum_{i=1}^{t} d_i^2$ is smallest, a least squares fit to the tangent plane is obtained. By Lagrange multiplier method the extreme value function is obtained:

$$L = \sum_{t=1}^{k} d_i^2 - \lambda\left(a^2 + b^2 + c^2 - 1\right) \tag{20}$$

Eq. (20) is obtained by taking the partial derivative of e and making the partial derivative zero:

$$\frac{\partial L}{\partial e} = 2\sum_{i=1}^{k}\left(ax_t + by_t + cz_t + e\right) = 0 \tag{21}$$

Eq. (19) and Eq. (21) can be solved by association:

$$d_i = \left|a\left(x_i - \bar{x}\right) + b\left(y_t - \bar{y}\right) + c\left(z_i - \bar{z}\right)\right| \tag{22}$$

Eqs. $\bar{x} = \frac{\sum_{t=1}^{k} x_i}{n}$, $\bar{y} = \frac{\sum_{i=1}^{k} y_i}{n}$, $\bar{z} = \frac{\sum_{i=1}^{k} z_r}{n}$. Substituting Eq. (22) into Eq. (20) and then taking the partial derivatives of a, b, and c respectively and making them equal to 0, we have:

$$\begin{cases} \frac{\partial L}{\partial a} = 2\sum_{t=1}^{i}\left(a\Delta x_t + b\Delta y_t + c\Delta z_i\right)\Delta x_t - 2\lambda a = 0 \\ \frac{\partial L}{\partial b} = 2\sum_{t=1}^{i}\left(a\Delta x_t + b\Delta y_t + c\Delta z_r\right)\Delta y_t - 2\lambda b = 0 \\ \frac{\partial L}{\partial c} = 2\sum_{i=1}^{i}\left(a\Delta x_t + b\Delta y_t + c\Delta z_i\right)\Delta z_i - 2\lambda c = 0 \end{cases} \tag{23}$$

where $\Delta x_t = x_i - \bar{x}$, $\Delta y_i = y_t - \bar{y}$, $\Delta z_i = z_i - \bar{z}$ are written in matrix form as:

$$AX = \begin{bmatrix} \sum_{i=1}^{i}\Delta x_t^2 & \sum_{i=1}^{i}\Delta x_t\Delta y_t & \sum_{i=1}^{i}\Delta x_t\Delta z_r \\ \sum_{i=1}^{i}\Delta x_i\Delta y_t & \sum_{t=1}^{i}\Delta y_t^2 & \sum_{i=1}^{i}\Delta y_t\Delta z_r \\ \sum_{t=1}^{i}\Delta x_t\Delta z_r & \sum_{t=1}^{i}\Delta y_t\Delta z_r & \sum_{i=1}^{i}\Delta z_t^2 \end{bmatrix}\begin{bmatrix} a \\ b \\ c \end{bmatrix} = \lambda\begin{bmatrix} a \\ b \\ c \end{bmatrix} = \lambda X \tag{24}$$

Since matrix A is a real symmetric matrix, it follows from knowledge of matrix theory:

$$\lambda=\frac{(AX,X)}{(X,X)}=\frac{a\left(a\sum_{i=1}^{1}\Delta x_i^2+b\sum_{i=1}^{i}\Delta x_i\Delta y_i+c\sum_{i=1}^{i}\Delta x_i\Delta z_i\right)}{a^2+b^2+c^2}$$
$$+\frac{b\left(a\sum_{i=1}^{i}\Delta x_i\Delta y_i+b\sum_{i=1}^{i}\Delta y_i^2+c\sum_{i=1}^{i}\Delta y_i\Delta z_i\right)}{a^2+b^2+c^2}$$
$$+\frac{c\left(a\sum_{1=1}^{i}\Delta x_1\Delta z_1+b\sum_{1=1}^{i}\Delta y_1\Delta z_1+c\sum_{1=1}^{i}\Delta z_i^2\right)}{a^2+b^2+c^2}$$
$$=\sum_{1=1}^{i}\left(a\Delta x_1+b\Delta y_i++c\Delta z_1\right)^2=\sum_{1=1}^{i}d_1^2 \tag{25}$$

When $S=\sum_{i=1}^{i}d_i^2$ is the smallest, the eigenvalue λ is also the smallest, and then the least squares fitting tangent plane can be obtained. That is, the eigenvector corresponding to the smallest eigenvalue of Eq. (24) is the normal vector of the least-squares tangent plane fitted to the k-neighbourhood point, and then the value of e can be obtained by substituting the coordinates of point p into Eq. (18).

2.3.2. Tangent plane projection Although the local region of the 3D point cloud can be approximated as a plane, the k-neighbourhood points of point p are not strictly located in the same plane, and it is necessary to project the k-neighbourhood points along the direction of the normal vector of the tangent plane onto the tangent plane. The k-neighbourhood point p coordinates after projection are calculated as:

$$p'_{project}=p_t-\frac{a(x_i-\bar{x})+b(y_s-\bar{y})+c(z_i-\bar{z})}{a^2+b^2+c^2}\cdot\begin{bmatrix}a\\b\\c\end{bmatrix} \tag{26}$$

2.3.3. Tangent plane rotation The tangent plane of point p is a plane in three-dimensional space, and the k-neighbourhood points projected onto the tangent plane are still essentially a set of points in three-dimensional space, which need to be further transformed to a two-dimensional plane. One method is to establish a local coordinate system at point p so that the z-coordinate values of the k-neighbourhood points in the local coordinate system are all 0. This method relies on the selection of orthogonal unit vectors and is not easy to compute. The schematic diagram of tangent plane rotation is shown in Fig. 1. In this paper, a more intuitive and easy-to-understand method is used, i.e., the normal vector of the tangent plane is rotated to be parallel to the z axes, i.e., the tangent plane of point p is rotated to be parallel to the xoy plane.

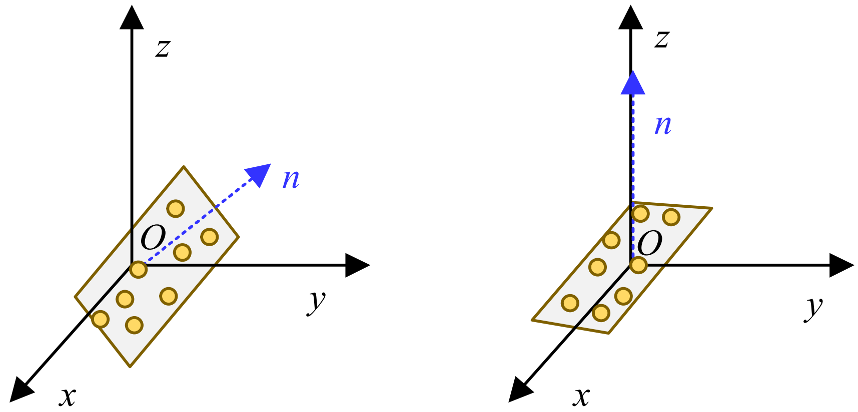

Fig. 1. The diagram of the tangent plane rotation

Let α be the tangent plane normal vector in the yoz-plane projection and the angle of the z-axis, β for the tangent plane normal vector in the yoz-plane projection and the tangent plane normal vector of the angle, (a,b,c) for the tangent plane normal vector calculated in the formula (24) n in the three-axis component of the normal vector, the normal vector rotation shown in Figure 2. First, the normal vector n around the x-axis counterclockwise rotation of α angles to the xoz-plane, and then the normal vector n around the y-axis counterclockwise rotation of β angles to parallel to the z-axis, this time the tangent plane parallel to the xoy plane.

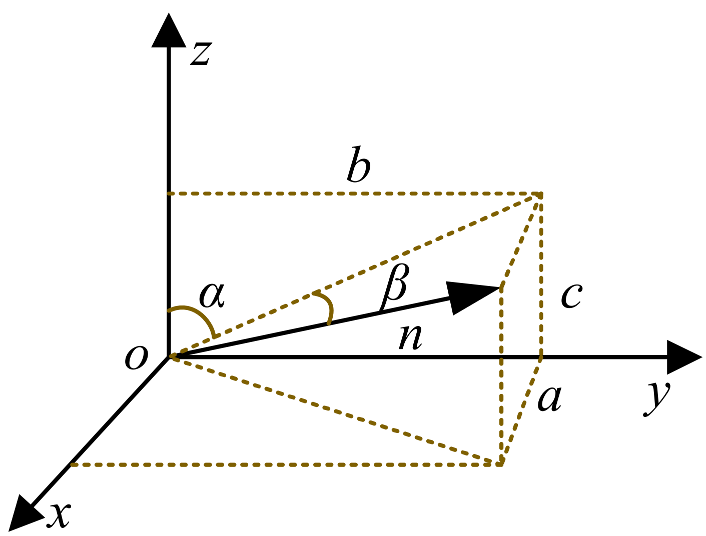

Fig. 2. The rotation of the normal vector

From the above, the rotation matrix is:

$$R = RR_x = \begin{bmatrix} \cos\beta & 0 & -\sin\beta \\ 0 & 1 & 0 \\ \sin\beta & 0 & \cos\beta \end{bmatrix} \begin{bmatrix} 1 & 0 & 0 \\ 0 & \cos\alpha & \sin\alpha \\ 0 & -\sin\alpha & \cos\alpha \end{bmatrix}$$
$$= \begin{bmatrix} s & 0 & -a \\ 0 & 1 & 0 \\ a & 0 & s \end{bmatrix} \begin{bmatrix} 1 & 0 & 0 \\ 0 & c/s & b/s \\ 0 & -b/s & c/s \end{bmatrix} \tag{27}$$

where $s = \sqrt{b^2 + c^2}$. Then the coordinates of the k -neighbourhood point in the plane parallel to the xoy -coordinate plane are:

$$\begin{bmatrix} x_t' \\ y_t' \\ z_t' \end{bmatrix} = R \begin{bmatrix} x_t \\ y_t \\ z_t \end{bmatrix} \tag{28}$$

The rotated k -neighbourhood point still has three coordinate values, but all the z -coordinate values are the same, so the subsequent processing directly discards the z -coordinate values and uses only the x, y -two coordinate values.

3. Analysis of the application effect of digital transformation in environmental art design innovation

3.1. *Performance analysis of 3D models in environmental art design*

In this paper, vs 2020 and OPENMVG are used to build an experimental platform to compare and analyse the execution speed and resultant matching effect of the camera self-calibration algorithm and SIFT algorithm proposed in this paper through experiments. In the experiment, the environmental art design images of several regions are compared with the UAV flights, and in the following, only two of the images collected by the UAV in two regions are selected as the experimental data, and the matching effect of two of the groups of images with the data obtained in the experimental process are listed.

3.1.1. Model data extraction and feature recognition performance analysis The experimental results of SIFT algorithm and camera self-calibration algorithm for feature matching of group A and group B data are shown in Table 1. The table lists the number of feature points extracted during the feature matching process, the feature point extraction time, the initial mis-matched point pairs and the initial matching time. It can be seen through the experimental comparative analysis that the feature point extraction time of the two groups of target images A and B of environmental art design using the camera self-calibration algorithm of this paper is reduced by 53.61% and 50.58%, respectively, compared with the SIFT algorithm, and the time used for feature point extraction is reduced by half compared with that of the traditional SIFT method. In addition, the initial number of mis-matched point pairs of the camera self-calibration algorithm for group A and group B is reduced by 324 pairs and 340 pairs respectively compared to the SIFT algorithm; and the initial matching time is reduced by 42ms and 67ms respectively.Obviously, compared with the traditional SIFT algorithm, the feature extraction in the digitally transformed environmental art design graphic is better by using the camera self-calibration algorithm in this paper.

Table 1. The experimental comparison of the two algorithms

Contrast feature		SIFT algorithm		Camera self-scaling algorithm	
		A group	B group	A group	B group
Characteristic	Original environmental art	21946	18492	21946	18492

point	design sheet				
	Target environmental art design sheet	20764	16985	20764	16985
Feature point extraction time(ms)	Original environmental art design sheet	52327	42208	23625	20108
	Target environmental art design sheet	49502	37404	22965	18486
Initial error matching point pair		5351	4649	5027	4309
Initial match time(ms)		273	224	231	157

The results of comparing the feature matching method (camera self-calibration algorithm) proposed in this paper with the basic matrix algorithm based on RANSAC are shown in Table 2. The table lists the number of correctly matched pairs of points, the number of mis-matched pairs of points, the mis-matching rate and the robust estimation time in the experiment. The results show that using the feature matching method proposed in this paper increases the number of correctly matched point pairs by 355 pairs and 216 pairs over the basic matrix algorithm based on RANSAC for group A and group B data, respectively; reduces the number of mis-matched point pairs by 355 pairs and 216 pairs, respectively; and reduces the mis-matching rate by 4.91% and 5.33%, respectively, and eliminates more incorrectly matched points. The robust estimation time (ms) time consumption is reduced by 147 ms and 128 ms, respectively.Obviously, the feature matching method proposed in this paper is more effective for the digital transformation of environmental art design.

Table 2. The two matrix estimation algorithm compares results

Contrast feature	Basic matrix algorithm based on RANSAC		Camera self-scaling algorithm	
	A group	B group	A group	B group
Correct match point pair	2887	2393	3242	2609
False match	2239	1933	2053	1693
False matching rate(%)	43.68	44.68	38.77	39.35
The robust estimation time (ms)	872	770	725	642

3.1.2. Gridded Test Results and Analysis. The relevant data of the meshing results are shown in Table 3. This paper mainly includes four related indicators, namely, the number of input point clouds (A), the number of triangles (B), the number of mesh vertices (C) and the surface area of the surface (D). As can be seen from the table, with the same number of input cloud points (112,171) for environmental art design under digital transformation, the mesh surfaces constructed by the Triangle Gridding Algorithm (TGA) proposed in this paper make greater use of the point cloud data.The number of triangles of the TGA method compared with the Rolling Ball Algorithm (BA) and the Traditional Region Growing Gridding Algorithm (TRGGA) increased respectively by 0.1797% and 0.1421%, the number of mesh vertices increased by 0.2967% and 0.3080%, and the surface area of the surface of the environmental art design increased by 29.15 cm^2 and 23.04 cm^2, respectively.In summary, the results of the triangular mesh algorithm based on the environmental art design proposed in this paper can maintain the basic shape of the model and the triangular mesh is more homogeneous, and it is able to clearly express the surface information of the environmental design model, and the mesh quality is improved. The triangular mesh algorithm proposed in this paper is better than the BA algorithm and TRGGA algorithm.

Table 3. Data on the grid results

Index	Triangular grid algorithm	Ball algorithm	Traditional regional growth grid algorithm
The number of input points	112171	112171	112171
Number of triangles	228983	224868	225730
Number of grid vertices	115797	112361	112231
Surface area(cm^2)	2836.21	2807.06	2813.17

3.2. Empirical study of digital transformation in environmental art design

3.2.1. Test indicators and test content. This paper takes the environmental art design of a museum constructed on the basis of 3D model as the research object, and evaluates the usability, functionality and acceptability of the overall interactive system based on 3D technology in the process of digital transformation of this museum. To verify the user's experience satisfaction and dissemination effect of digital transformation innovation and practice based on environmental art design. The results of the indicator description of the user subjective evaluation scale are shown in Table 4. Two assessment items, task testing and filling out the subjective evaluation scale, were carried out separately for the target users. The evaluation indicators are based on the five usability evaluation dimensions of ease of learning, efficiency, memorability, fault tolerance and satisfaction proposed by Nielsen, and combined with the three indicators of cognition, psychology, attitude and behaviour used in communication studies to study communication effects, and are finally summarized into three first-level indicators and nine second-level indicators. After completing the task test, users filled in a subjective evaluation scale to rate each indicator, with a score from 1 to 5, with 5 being very satisfied and 1 being very dissatisfied. The testing time for each user was no more than 60 minutes.

1) Test user selection. Regarding the number of users to be recruited, 200 representative users interested in museums, aged between 21-35, able to use mobile phones proficiently, and with a certain understanding or experience of 3D modelling digital transformation technology in the process of environmental art design, were selected for the sub-test.

2) Test task content. The user task test is divided into two parts: interface operation and actual experience of AR function, and the task design is centred around the core functions of innovative practice and application of environmental art design for digital transformation.

Table 4. User subjective evaluation scale

Primary indicator	Secondary indicator	Index description
Interface availability	B1:Visual style	The overall style is harmonious and beautiful
		The icon design is reasonable and easy to understand
	B2:Interactive operation	The functional level is clear and the operation process is reasonable
		The gesture operation is in line with the daily usage
	B3:Emotional experience	The overall experience satisfied me
3D scene experience	B4:Functionality	I can clearly view the details of the artifacts and meet my expectations
	B5:Availability	Easy to operate and quick to handle
	B6:Pleasure	I enjoy the experience, it's fascinating
Innovation and dissemination of digital transformation	B7:Cognition	The presentation is both informative and easy to understand
		The form of the literature and exhibition is novel and interesting
	B8:Psychology and attitude	I am willing to contact this form of communication
		I think this form has artistic appeal and has a positive effect on cultural communication
	B9:Behavior	I think that's a strong sense of participation
		I am willing to focus on relevant information

3.2.2. Test results and analyses. The results of subjective evaluation of satisfaction with secondary indicators are shown in Figure 3. The results of the survey can be obtained that the average satisfaction ratings of the subjects on the secondary indicators from B1-B9 are 4.45, 4.95, 4.75, 4.18, 4.70, 4.60, 4.44, 4.50, and 4.40, respectively, and the average scores of all the secondary indicators are all above 4. It is obvious that the overall satisfaction of users with the digital transformation application of 3D models in the environmental art design process of this museum is high. Among them, the interactive operation score is more prominent (4.95), and users are more satisfied with the design of various types of gestures, which is in line with daily use habits. The functionality of the 3D model digital transformation score is lower (4.18), the reason for this is mainly due to the limitations of their own technical level, the 3D model digital transformation function experience failed to combine with the application interface interaction prototype, making its display more simple resulting in a lower score. From a comprehensive point of view, the museum's 3D model digital transformation application basically meets the user's expectations. Visually achieve beautiful atmosphere, functionally meet the basic display of cultural relics at the same time, through the three-dimensional model digital transformation technology to a certain extent to enhance the user experience of pleasure and immersion. Better achieve the collection of cultural resources in the process of environmental art design digital display and dissemination, the digital transformation process of environmental art design innovation and dissemination is of great significance.

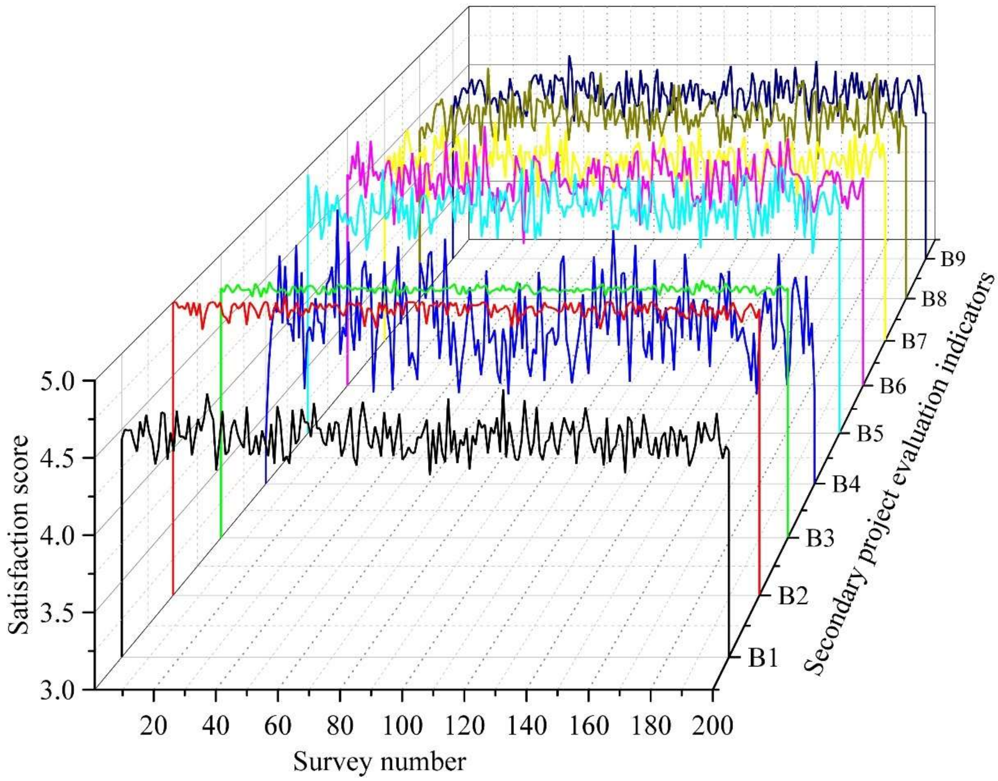

Fig. 3. The subjective evaluation results of the secondary index satisfaction

4. Conclusion

This paper proposes a 3D reconstruction algorithm for irregular shapes. The digital transformation of images in the process of environmental art design is discussed in detail and experimentally verified from the aspects of image acquisition, feature extraction, feature matching and 3D reconstruction. The results show:

1) the feature point extraction time of A and B target images of environmental art design using this paper's camera self-calibration algorithm is reduced by 53.61% and 50.58% compared with the SIFT algorithm, respectively; the number of initial mis-matched point pairs is reduced by 324 pairs and 340 pairs, respectively; and the initial matching time is reduced by 42ms and 67ms, respectively. in addition, using this paper's feature matching method can increase the number of data of correctly matched point pairs (355 pairs and 216 pairs), reduce the number of mis-matched point pairs (355 pairs and 216 pairs), decrease the mis-matching rate (4.91% and 5.33%), save the time consumption (147ms and 128ms), and eliminate more incorrectly matched points. Obviously, using the algorithm in this paper is better for environmental art design graphics in in digital transformation.

2) In the case of the same number of cloud points in the environmental art design input (112,171), the mesh surface constructed by the triangle meshing algorithm proposed in this paper makes greater use of the point cloud data. Compared with other methods, the number of triangles, the number of mesh vertices, and the surface area of the surface increased by 0.1797%-0.1421%, 0.2967%-0.3080%, and 29.15 cm^2-23.04 cm^2, respectively, and the triangular mesh is more uniform, which can clearly express the surface of the environmental design model. Clearly express the surface information of the environmental design model, and the mesh quality is improved.

3) Taking the 3D reconstruction results of a museum scene as an example, the subjects' satisfaction scores for the secondary indicators from B1-B9 are all greater than 4, which shows that the overall

satisfaction of the users with the application of digital transformation of 3D models in the process of environmental art design is higher.

References

[1] Yang, Y., & Dan, Z. (2020). Environmental design vs. Environmental art design: a Chinese perspective. TARIH KÜLTÜR VE SANAT ARAşTıRMALARı DERGISI, 9(4), 122-133.

[2] Zhuoyu, G. (2023). The Relationship between Urban Public Space Reconstruction and Environmental Art Design. Journal of Civil Engineering and Urban Planning, 5(9), 49-53.

[3] Li, P., Liu, K., & Chen, F. (2024). Cognitive characteristics of concept derivation phase in environmental art design: A epistemic network analysis of design scheme construction process. The Design Journal, 1-21.

[4] Wei, Y. (2016, March). Environmental Art Design Based on Ecological Philosophy Perspective. In 2016 International Conference on Education, Sports, Arts and Management Engineering (pp. 274-278). Atlantis Press.

[5] Gong, P. (2023). Landscape art design of public environment based on the concept of sustainable development. Computer-Aided Design and Applications, 21(S2), 113-125.

[6] Wenhui, Y. (2017). Reconstruction and paradigm of the thinking mode of environmental art design. International Journal of Technology, Management, 214-219.

[7] Gui, S. (2021, April). Research on the Innovation and Development of Environmental Design curriculum in the context of Informatization. In 2021 International Conference on Internet, Education and Information Technology (IEIT) (pp. 217-221). IEEE.

[8] Jin, H., & Yang, J. (2021). Using computer-aided design software in teaching environmental art design. Computer-Aided Design and Applications, 19(S1), 173-183.

[9] Shen, Y., & Yu, F. (2021). The influence of artificial intelligence on art design in the digital age. Scientific programming, 2021(1), 4838957.

[10] Luo, K., & Dong, L. (2021, May). Research on the application of environmental art design based on digital media technology. In Journal of Physics: Conference Series (Vol. 1915, No. 2, p. 022072). IOP Publishing.

[11] Posthumus, S., Sinclair, S., & Poplawski, V. (2018). Digital and environmental humanities: strong networks, innovative tools, interactive objects. Resilience: A Journal of the Environmental Humanities, 5(2), 156-171.

[12] Lyytinen, K. (2022). Innovation logics in the digital era: a systemic review of the emerging digital innovation regime. Innovation, 24(1), 13-34.

[13] Zhanjun, W. (2017). Application research of virtual reality technology in environmental art design. Acta Technica CSAV (Ceskoslovensk Akademie Ved), 62(1), 215-224.

[14] Xu, B., Yu, T., & Zhou, S. (2020). Teaching design and practice based on the dissemination of professional knowledge in digital media environment art design. IEEE Access.

[15] Liu, P., Song, C., Ma, X., & Tang, X. (2022). Visual Space Design of Digital Media Art Using Virtual Reality and Multidimensional Space. Mobile Information Systems, 2022(1), 8220572.

[16] Liu, C. (2021, August). Research on urban public art design based on digital information technology. In Journal of Physics: Conference Series (Vol. 1992, No. 2, p. 022081). IOP Publishing.

[17] Hu, J., & Fu, L. (2022). Innovation and Development of environmental art design thinking based on artificial intelligence in culture, form and function. In International Conference on Cognitive based Information Processing and Applications (CIPA 2021) Volume 1 (pp. 635-642). Springer Singapore.

[18] Jacobs, R., & Leal, S. (2018). Digital participation through artistic Interventions. In Digital Participation through Social Living Labs (pp. 37-54). Chandos Publishing.

[19] Esposito, M. A., & Bosi, F. (2021). The Green Design Approach Digital Innovation Facility: BIM and New Industrial Processes. Bioclimatic approaches in urban and building design, 439-485.

[20] Marks, M., Chandler, L., & Baldwin, C. (2017). Environmental art as an innovative medium for environmental education in Biosphere Reserves. Environmental Education Research, 23(9), 1307-1321.

[21] Donatas Gurauskis, Dalius Mažeika & Artūras Kilikevičius. (2024). Self-calibratable absolute modular rotary encoder: a theoretical feasibility study. Measurement Science and Technology(12),125108-125108.

[22] Patrick Tritschler, Torsten Ohms, Bin Yang & André Zimmermann. (2024). Meta-learning for few-shot sensor self-calibration to increase stress robustness. Engineering Applications of Artificial Intelligence(PA),109171-109171.

[23] Yang Ruiqi, Zhang Junhua & Li Bo. (2023). An end-to-end convolutional network for estimating the essential matrix. Image and Vision Computing

[24] Pei Yi Wu & Ling Yang. (2024). The rigidity of minimal Legendrian submanifolds in the Euclidean spheres via eigenvalues of fundamental matrices. Calculus of Variations and Partial Differential Equations(8),217-217.

[25] Ai Guo Wu, Yu Tian Xu & Jie Mei. (2024). State Responses of Several Classes of Linear Systems Based on Fundamental Matrices.. IEEE transactions on cybernetics

[26] Teng Fei Zhu, Yang Liu, Zhi Luo & Xiao Ping Ouyang. (2024). Sparse-view neutron CT 3D image reconstruction algorithm based on split Bregman method. Nuclear Science and Techniques(9),152-152.

[27] S.Delgado Díez, C.Cerrada Somolinos & S. R.Gómez Palomo. (2024). Optimizing Surface Voxelization for Triangular Meshes with Equidistant Scanlines and Gap Detection. (Computer Graphics Forum(6),e15195-e15195.